Directional allosteric regulation of protein filament length

Adam S. Jermyn,[1,2] Wenxiang Cao,[3] W. Austin Elam,[3,*] Enrique M. De La Cruz,[3] and Milo M. Lin[2]

[1]*Center for Computational Astrophysics,Flatiron Institute, New York, New York, 10010, USA*
[2]*Green Center for Molecular, Computational, and Systems Biology, University of Texas Southwestern Medical Center, Dallas, Texas 75390, USA*
[3]*Department of Molecular Biophysics and Biochemistry, Yale University, New Haven, Connecticut 06511, USA*

Cofilin and ADF are cytoskeleton remodeling proteins that cooperatively bind and fragment actin filaments. Bound cofilin molecules do not directly interact with each other, indicating that cooperative binding of cofilin is mediated by the actin filament lattice. Cofilactin is therefore a model system for studying allosteric regulation of self-assembly. How cofilin binding changes structural and mechanical properties of actin filaments is well established. Less is known about the interaction energies and the thermodynamics of filament fragmentation, which describes the collective manner in which the cofilin concentration controls mean actin filament length. Here, we provide a general thermodynamic framework for allosteric regulation of self-assembly, and we use the theory to predict the interaction energies of experimental actin filament length distributions over a broad range of cofilin binding densities and for multiple cofilactin variants. We find that bound cofilin induces changes in nearby actin-actin interactions, and that these allosteric effects are propagated along the filament to affect up to four neighboring cofilin-binding sites (i.e., beyond nearest-neighbor allostery). The model also predicts that cofilin differentially stabilizes and destabilizes longitudinal versus lateral actin-actin interactions, and that the magnitude, range, asymmetry, and even the sign of these interaction energies can be altered using different actin and cofilin mutational variants. These results demonstrate that the theoretical framework presented here can provide quantitative thermodynamic information governing cooperative protein binding and filament length regulation, thus revealing nanometer length-scale interactions from micron length-scale "wet-lab" measurements.

I. INTRODUCTION

Self-assembly of nanoscale proteins into micronscale filaments is one of the most common yet consequential behaviors in molecular biology. Protein filaments are implicated in the majority of neurodegenerative diseases, most notably the cross-β amyloid fibril associated with Alzheimer's disease [1]. Yet protein self-assembly into one-dimensional filaments is also necessary for biological function. The most common example is actin, which constitutes the cytoskeleton of cells, drives cellular motion, and forms the synaptic structures that allow neuronal communication [2,3]. A suite of auxiliary regulatory proteins further control actin filament length, localization, cross-linking, and branching [4]. These regulatory molecules bind to actin monomers in the filament. This binding interaction can alter the conformational preference of actin, thereby affecting actin-actin (i.e., filament) stability in the vicinity of regulatory binding. This phenomenon, whereby interactions in one part of a protein affects the behavior of a distant part of the protein or adjacent proteins, is called allostery, and it is a pervasive property allowing for the conditional activation of protein function and self-assembly.

In the case of actin, allostery extends the effects of regulatory proteins beyond the locality of their direct binding with the actin filament, giving rise to longer-range coupling.

The presence of such coupling is inferred from experimental measurements of atomistic structural changes as well as "macroscopic" filament length distributions. However, structural studies are indirect probes of allostery; it is difficult to infer, based on structure, the magnitude or sign of the changes in interaction energies, and energetic or entropic effects could propagate in the absence of discernable structural change [5,6]. How structural perturbations are related to interaction energies, and how these molecular-scale energetics collectively regulate cell-scale effects, are open questions.

One-dimensional order-disorder transitions, and reversible filament self-assembly from monomeric subunits, are both well-established theoretically. Exact transfer matrix-based calculations of Ising partition functions have led to analytically tractable insights into biological processes such as the helix-to-coil transition in proteins [7]; recently, this approach has been extended to multi-component systems, with allosteric effects limited to nearest neighbor (spin-spin) interactions [8]. Self-assembly in the absence of allosteric regulation has also been analytically solved in the case of identical monomers [9]. Here, we extend and combine these approaches to create a framework for predicting the equilibrium length distribution for arbitrary allosteric self-assembly Hamiltonians, and apply it to study actin assembly and modulation by regulatory proteins. The framework models an ensemble of linear polymers (e.g., actin filaments) within which an allosteric interaction Hamiltonian is integrated in

* Current address: C4 Therapeutics, Cambridge, MA 02142, USA.

a modular fashion via a generalized Ising model, thereby allowing for exact analytic calculation of the filament length distribution as a function of any regulatory component interaction. The model is general, and applicable to any linear polymer with any type of allosteric interactions, both with and without associated regulatory components. The theory is also analytically solvable, enabling comprehensive fitting over the entire parameter space for any type of allosteric regulation.

Application of this model to the experimentally measured cofilactin filament length distribution, measured for three different actin and cofilin variants (isoforms), yields in all cases a single unique best fit following exhaustive enumeration over the parameter space. The results show that cofilin binding to an actin filament changes actin-actin interaction energies up to four repeat units away from the binding site. Depending on the variant, these allosteric effects can propagate symmetrically or asymmetrically from the binding site. The analysis also shows that cofilin binding in most variants destabilizes lateral contacts, but either stabilizes or has weak effect on longitudinal filament interfaces, consistent with molecular dynamics simulations [10] and structural signatures from experiments carried out with purified protein components [11–13]. The statistical mechanical framework presented here thus provides quantitative thermodynamic information governing allosteric length regulation of actin filaments, and shows how genetic variation can tune allosteric interactions.

II. THEORY

A. General Model of Linear Polymer Self-Assembly

The theoretical length distribution of one-dimensional equilibrium self-assembly in the absence of regulation or allostery has been solved [9]. Here, we extend this framework to allow for allosteric regulation. We consider a system composed of $N \gg 1$ identical molecules at constant temperature T and in a solution of constant unit volume V. These molecules polymerize (i.e., self-assemble), forming linear filaments, with the interactions between the molecules possibly being allosteric in nature, as well as regulated by other types of molecules at fixed concentration. Polymerization occurs in the dilute limit, where the total protein and polymer occupied volume (V_{occ}) is much less than the solvent volume ($V_{occ} \ll V$) and, thus, interactions between filaments are negligible. In this limit the free energy of each polymer becomes extensive in its length. The concentration of filaments of length L is then given by

$$c_L = e^{-\gamma - \kappa L}. \tag{1}$$

Here γ is the free energy of creating a new filament (i.e., the filament scission energy) and κ is the free-energy change associated with adding one more monomer to a filament [14]. By minimizing the free energy corresponding to the dilute limit partition function subject to the constraint of fixed total monomer concentration, the change in free energy associated with adding a monomer to a filament may be related to the filament scission energy by

$$\kappa = -\ln\left(1 + \frac{1 - \sqrt{1 + 4ce^{\gamma}}}{2ce^{\gamma}}\right). \tag{2}$$

The distribution specified by Eqs. (1) and (2) may be used to extract any moment of interest. An experimentally

accessible moment is the mean filament length

$$\langle L \rangle = \frac{\sum_{L=1}^{N} L c_L}{\sum_{L=1}^{N} c_L} = \frac{1}{1 - e^{-\kappa}}. \tag{3}$$

This only depends on κ, which in turn depends only on the effective filament nucleation term γ. Note that Eqs. (2) and (3) hold regardless of the type of (possibly allosteric) interactions, with γ computed from the interaction Hamiltonian (e.g., see below for actin self-assembly regulated by cofilin). In the special case of nonregulated and nonallosteric self-assembly with monomer-monomer binding free energy J, $\gamma = J$. Inserting Eq. (2) into Eq. (3) then yields

$$\langle L \rangle = \frac{1}{2}\left[1 + \sqrt{1 + 4ce^{\beta J}}\right], \tag{4}$$

which is the known result for simple self-assembly [9]. In the low concentration limit such that most monomers are unbound, in setting the critical nucleation size $n = 2$ and assuming the nucleation rate constant is equal to that of monomer addition (i.e., $k_n = k_+$), Eq. (1) simplifies to

$$c_L = \frac{k_n}{k_-} c_1^2 \left(\frac{k_+}{k_-} c_1\right)^{L-2} \tag{5}$$

the classic result [15,16] for the case in which filament fragmentation and annealing can be ignored [17], which is simply modified if the critical nucleus is a trimer [18,19]. Incorporating higher-order corrections due to intrachain interactions and nucleation effects in the very long ($L \gg L_p$) and very short ($L \ll L_p$), regimes, respectively, is straightforward. The conformational entropy has a power-law scaling with length, which may be inserted into Eq. (1) as a modification to κ. Similarly, nucleation effects can be incorporated by treating the case of $L = 1, 2$ separately and then only using Eq. (1) for longer filaments.

The model in Eqs. (1) and (2) applies more generally to self-assembly regulated by additional molecules in the presence of allosteric interactions. In that case, we need to introduce a Hamiltonian to capture such interactions. With such a Hamiltonian we can compute the associated partition function to obtain κ and γ. This results in a new length distribution following Eq. (1) but with energies determined by the physics of the additional degrees of freedom.

III. ACTIN ASSEMBLY REGULATED BY COFILIN

Cofilin molecules bound to actin filaments do not directly interact [20], indicating that the cooperative interactions between cofilin propagate allosterically from occupied sites to vacant sites in the filament. Long-range destabilizing effects of bound cofilin have been implicated in filament depolymerization and fragmentation (see, e.g., Refs. [11,21]). The reported length over which cofilin-linked conformational changes propagate along actin filaments varies dramatically, ranging from 1 to 3 [22,23] up to $\sim$100 filament subunits [11,21], and may be directionally asymmetric [24,25]. A recent electron cryomicroscopy study [23] suggests that changes in filament twist are effectively local and propagate allosterically only over 1–3 subunits, but with one side (pointed end directed) appearing to be slightly longer-range (2 or 3 subunits) than the other (barbed end directed).
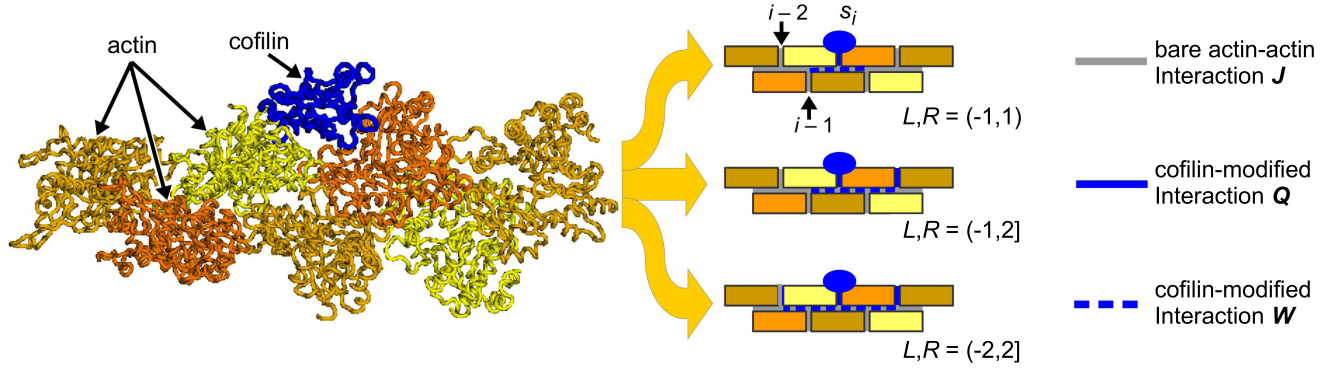
FIG. 1. Potential effects of cofilin occupancy on actin filament interfaces. Actin filament subunits, shown in different shades of yellow in structure image at left and represented by bricks in the model at right, are held together by longitudinal and lateral intermolecular interactions J, represented by gray interfaces. Cofilin (blue) binding within a longitudinal subunit interface is associated with a binding free energy (chemical potential P) and modulation of neighboring, longitudinal (Q) and lateral (W) actin subunit interfaces (represented by solid and dashed blue, respectively). Note the use of square brackets versus parentheses to denote whether an edge Q-interaction is included.

We built a Hamiltonian for cofilin regulation of actin filament, accounting for the energetic contributions from actin filament extension, direct cofilin binding, and local conformational changes of actin filament induced allosterically by cofilin binding. The model is essentially a grand canonical ensemble for a filament of length L and fixed cofilin binding saturation, which we match to experimental conditions using an effective binding coefficient P (see below and Materials and Methods). We map double strand actin filament with allosteric regulation to a generalized Ising model for the binding occupancy of the regulatory protein (Fig. 1). We use i to index actin ("bricks" in Fig. 1) as well as its associated cofilin-binding sites (positioned at interface between longitudinal filament actin subunits i and $i-2$). We use the variable s_i to track whether or not cofilin is bound at each site: $s_i = 1$ if bound to cofilin, and $s_i = 0$, otherwise.

When no cofilin is bound to the polymer, its energy is just set by the unmodified actin-actin binding energy J. So,

$$H_0 = -J(1-L). \qquad (6)$$

The direct actin-cofilin binding interaction energy is given by $-\lambda$ for each bound cofilin. However, cofilin binding has a chemical potential μ, such that the free energy increases by μ when a cofilin molecule binds to an actin filament. We may combine these into an effective binding coefficient P given by

$$P = -\mu + \lambda. \qquad (7)$$

This produces a term in the Hamiltonian of the form

$$H_{\text{direct}} = -P \sum_i s_i. \qquad (8)$$

When cofilin binds to an actin filament it also induces conformational changes at the neighboring actin subunits (i, i-2). This is shown in Fig. 1, where a bound cofilin molecule is denoted by a blue oval. These conformational changes in turn modulate the binding energy of those actin subunits to their neighbors. To account for these effects we introduce two interaction energies Q and W. The former accounts for changes in the in-plane actin-actin binding energy

(e.g., i interacting with $i+2$), and is of the form

$$H_{\text{in-plane}} = -Q \sum_i \left[1 - \prod_{j \in M}(1 - s_{i-j}) \right]. \qquad (9)$$

The set

$$M = \{i | \mathcal{L} \leqslant i \leqslant \mathcal{R}, i = 0 \,(\text{mod}2)\} \qquad (10)$$

constrains the longitudinal coupling (Q) to neighbors in the same plane with separations between $\mathcal{L}$ and $\mathcal{R}$. When $Q > 0$ the net impact of this term is to enforce the energy of all in-plane actin-actin bonds within the specified range of a bound cofilin molecule, i.e., to stabilize/favor longitudinal actin assembly. When $Q < 0$ this term has the opposite effect, indicating that bound cofilin destabilizes or is unfavorable to longitudinal actin assembly.

The remaining interaction W behaves similar to Q and accounts for changes in the out-of-plane actin-actin binding energy (e.g., i interacting with $i+1$). Its contribution is given by

$$H_{\text{out-of-plane}} = -W \sum_i \left[1 - \prod_{j=\mathcal{L}}^{\mathcal{R}}(1 - s_{i-j}) \right]. \qquad (11)$$

When $W > 0$ the net impact of this term is to strength the energy of all out-of-plane actin-actin bonds within the specified range of a bound cofilin molecule and to stabilize lateral actin assembly. When $W < 0$ this term has the opposite effect.

Putting together the various different energy terms, we arrive at a Hamiltonian of the form

$$H = -J(1-L) - P \sum_i s_i - Q \sum_i \left[1 - \prod_{j \in M}(1 - s_{i-j}) \right]$$
$$-W \sum_i \left[1 - \prod_{j=\mathcal{L}}^{\mathcal{R}}(1 - s_{i-j}) \right], \qquad (12)$$

where now we may work just in the canonical ensemble for a given filament length L because the effects of cofilin

concentration are incorporated into P due to the one-to-one mapping between binding and cofilin-actin interactions. This form is useful because the experimentally available parameter is the cofilin binding fraction on the polymers, which we may use to directly compute P but not μ or λ [26,27].

The range and asymmetry of change in actin-actin interaction energy induced by cofilin binding correspond to different values of the ranges between $\mathcal{L}$ and $\mathcal{R}$. These introduce different effective coupling functions between actin subunits and bound cofilins, and generate different equilibrium filament length distributions. The range and asymmetry of the allosteric interactions are given by

$$\text{Range} \equiv \mathcal{R} - \mathcal{L} \tag{13}$$

and

$$\text{Asymmetry} \equiv \mathcal{R} + \mathcal{L}. \tag{14}$$

Note that the Range refers to the distance between two cofilin binding sites ($i + \mathcal{L}$ and $i + \mathcal{R}$), not the number of cofilin binding sites in the Range. Within the Range, all the lateral actin-actin interfaces and those longitudinal actin-actin interfaces on the same protofilament strand are affected by a cofilin binding. Therefore, the Range and Asymmetry depict how induced changes at the actin-actin interface spread. For example, $(\mathcal{L}, \mathcal{R}) = (-1, 2]$, the second case in Fig. 1, has Range = 3. Within the distance between cofilin binding sites $i - 1$ and $i + 2$, 3 lateral (actin $i - 2$ interacting with $i - 1$; $i - 1$ with i; i with $i + 1$) and 2 longitudinal actin-actin interfaces (actin $i - 2$ with i; and i with $i + 2$) are modified by a cofilin binding at site i, as shown in blue in Fig. 1. This case has an Asymmetry = 1, indicating one more lateral actin-actin interface changed on the right side than on the left side of the bound cofilin.

Because the Hamiltonians of candidate interactions [Eq. (12)] is symmetric with respect to left and right, our model is fully characterized by the Range and Asymmetry. We also explore permutations of Eq. (10) in which one or both of the inequalities are noninclusive; the former case breaks the directional symmetry. The difference between an inclusive (denoted by a square bracket) and noninclusive (denoted by a parenthesis) is including or not including a possible longitudinal Q term on the edge of the range spanned by the lateral interactions W (dashed blue line in Fig. 1). For example, for $L, R = -1, 2$, $(-1, 2]$ means to include the Q term at the edge $i + 2$, whereas $(-1, 2)$ excludes the Q term at that edge. However, because there is no Q term at the edge $i - 1$, there is no difference between inclusive and noninclusive notations $(-1, 2)$ and $[-1, 2)$. As we shall see, the models in which one side of the Q term is noninclusive fit as well or better than the fully inclusive model, so we focus on the former in the remainder of this work (Figs. 2–5 and Table I). Fits that focus on the latter are presented in Fig. 6 and agree with the conclusions derived from the former.

IV. MATERIALS AND METHODS

A. Chemicals and protein purification

All buffer chemical reagents were the highest purity commercially available and purchased from American Bioanalyti-
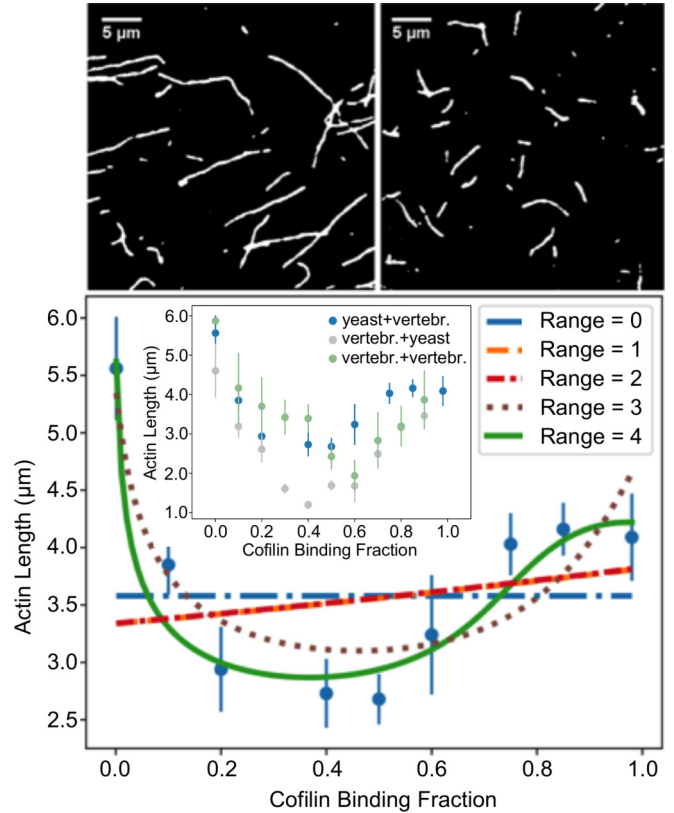

FIG. 2. Cofilin modulates nonnearest neighbor actin filament interfaces. Top: representative TIRF microscopic images of actin filaments at a cofilin binding density of 0 (left, long filaments) and 0.5 (right, short filaments). Bottom inset: raw experimental data for all three mutational isoforms. Bottom: the measured mean filament length (blue circles)-dependence on the cofilin binding density for RSKactin (vertebrate) actin at 2 μM with varying saturation of yeast cofilin D34CyCof. The best fits for different ranges (Range = 0, 1, 2, 3, or 4) and maximum asymmetry of allostery are indicated by the continuous lines through the data. The best fit at each range is over all possible asymmetries as well as all possible parameters for each asymmetry. The best Range 3 ([0, 3]; qualitative matching; purple dotted line) fit allosteric parameters are (in units of kT): $J = -9.9$, $Q = -0.8$, $W = 1.0$. The best Range 4 ([0, 4] or (0, 4]; quantitative matching; green sold line) fit values are: $J = -10.1$, $Q = -1.1$, $W = 1.5$. Note that these curves are independent of actin concentration and can be rescaled with a scaling factor.

cal or Sigma-Aldrich. Rabbit skeletal muscle actin (RSKactin) and Yeast actin A167E was purified and labeled with Alexa 488-succimidyl ester (Molecular Probes, Eugene, OR) [27]. Actin monomers with bound Ca^{2+} were converted to Mg^{2+}-actin by addition of 200 μM EGTA and $MgCl_2$ at a concentration equal to the total actin concentration plus 40 μM immediately before polymerization. Actin was polymerized by addition of 0.1 volume of $10\times$ polymerizing salt solution yielding actin filaments in "polymerization buffer" (50 mM KCl, 2 mM MgCl2, 0.2 mM ATP, and 10 mM imidazole, pH 6.8) supplemented with freshly dissolved DTT (2 mM) and equilibrated at room temperature for ~1 h. Human cofilin 1 (hCof) and *Saccharomyces cerevisiae* D34C mutant cofilin (D34CyCof) were purified as described [28].

TABLE I. The fit parameters for each model run are shown along with 1-σ uncertainties, denoted by the prefix "d" in each of the positive (+) and negative (−) directions.

Actin	Cofilin	L	R	Both inclusive?	Q	$dQ-$	$dQ+$	W	$dW-$	$dW+$	J	$dJ-$	$dJ+$	Reduced χ^2
RSKactin	D34C_yCof	0	4	False	1.09	0.3	0.3	−1.46	0.3	0.26	10.07	0.2	0.18	1.63
RSKactin	D34C_yCof	−4	0	True	−0.67	0.19	0.18	−0.44	0.25	0.23	9.98	0.18	0.18	2.28
RSKactin	D34C_yCof	0	4	True	−0.67	0.22	0.19	−0.23	0.13	0.12	9.99	0.19	0.19	2.32
RSKactin	D34C_yCof	−1	3	False	0.1	0.67	0.67	−0.85	0.29	0.28	10.15	0.18	0.17	2.79
RSKactin	D34C_yCof	−1	3	True	0.07	0.73	0.68	−0.86	0.31	0.29	10.15	0.18	0.19	2.81
RSKactin	D34C_yCof	0	3	False	0.84	0.16	0.16	−0.97	0.13	0.13	9.89	0.19	0.18	3.47
RSKactin	D34C_yCof	−2	2	True	−1.33	0.49	0.5	−0.36	0.33	0.25	9.76	0.16	0.19	3.58
RSKactin	D34C_yCof	−4	0	False	−1.12	0.44	0.42	−0.52	0.25	0.25	10.01	0.17	0.16	3.73
RSKactin	D34C_yCof	−2	2	False	−1.17	0.51	0.44	−0.54	0.3	0.26	10.02	0.17	0.19	3.77
RSKactin	D34C_yCof	−1	2	True	−1.18	0.56	0.51	−0.38	0.26	0.26	9.96	0.18	0.17	4.16
RSKactin	D34C_yCof	−1	2	False	−1.16	0.56	0.5	−0.39	0.26	0.26	9.97	0.18	0.17	4.16
RSKactin	D34C_yCof	−3	1	True	−1.75	0.35	0.35	−0.2	0.23	0.24	9.89	0.18	0.17	4.47
RSKactin	D34C_yCof	−3	1	False	−1.75	0.36	0.35	−0.2	0.23	0.24	9.89	0.18	0.17	4.47
RSKactin	D34C_yCof	0	3	True	−1.64	0.46	0.42	−0.11	0.13	0.14	9.91	0.18	0.17	4.48
RSKactin	D34C_yCof	−3	0	True	−1.71	0.4	0.35	−0.2	0.25	0.26	9.89	0.18	0.17	4.5
RSKactin	D34C_yCof	−3	0	False	−1.74	0.49	0.38	−0.23	0.3	0.27	9.91	0.19	0.2	4.51
RSKactin	D34C_yCof	−2	0	True	−2.01	0.37	0.32	0.08	0.24	0.22	9.79	0.19	0.18	4.65
RSKactin	D34C_yCof	0	2	True	−1.93	0.42	0.36	−0.01	0.12	0.13	9.82	0.19	0.18	4.66
RSKactin	D34C_yCof	−2	1	True	−1.92	0.39	0.79	−0.01	1.43	0.26	9.84	0.22	0.29	4.74
RSKactin	D34C_yCof	−2	1	False	0.08	4.11	4.04	−0.88	0.23	0.24	9.69	0.21	0.2	7.78
RSKactin	D34C_yCof	−1	1	False	0.03	4.05	4.02	−0.92	0.22	0.26	9.78	0.25	0.23	8.03
RSKactin	D34C_yCof	−1	1	True	−0.02	4.04	4.1	−0.92	0.23	0.25	9.78	0.25	0.23	8.03
RSKactin	D34C_yCof	0	2	False	0.03	3.96	4.02	0.13	4.03	3.97	8.78	0.16	0.16	8.31
RSKactin	D34C_yCof	0	0	True	−0.1	4.05	4.16	0.05	4.1	4.02	8.95	0.07	0.06	8.51
RSKactin	D34C_yCof	0	0	False	−0.01	4.06	4.07	−0.07	4.07	4.13	8.95	0.07	0.07	8.51
RSKactin	D34C_yCof	−1	0	True	0.05	4.13	4.07	0.41	0.31	0.3	8.74	0.16	0.17	9.62
RSKactin	D34C_yCof	−1	0	False	0.02	4.08	4.06	0.42	0.32	0.3	8.74	0.16	0.17	9.62
RSKactin	D34C_yCof	0	1	True	0.12	4.16	4.02	0.16	0.14	0.14	8.78	0.16	0.16	9.7
RSKactin	D34C_yCof	0	1	False	0.01	4.07	4.08	0.16	0.14	0.14	8.78	0.16	0.16	9.7
RSKactin	D34C_yCof	−2	0	False	−0.05	4.04	4.13	−0.25	0.28	0.27	9.12	0.2	0.19	9.79
RSKactin	hCof	−1	1	False	0.01	4.1	4.09	−1.46	0.12	0.11	9	0.03	0.03	1.51
RSKactin	hCof	−1	1	True	0.03	4.11	4.06	−1.47	0.11	0.11	9	0.03	0.03	1.51
RSKactin	hCof	−2	1	False	−0.27	3.83	4.28	−1.74	0.2	0.15	9.02	0.04	0.04	1.57
RSKactin	hCof	−2	0	False	−0.03	4.05	4.12	−2.1	0.18	0.17	8.99	0.03	0.03	1.64
RSKactin	hCof	−1	3	False	−3.34	1.2	2.29	0.17	0.73	0.23	9.02	0.04	0.04	1.64
RSKactin	hCof	−1	3	True	−3.28	1.23	2.43	0.16	0.8	0.24	9.02	0.04	0.04	1.66
RSKactin	hCof	0	2	False	−0.66	3.65	3.65	−0.67	3.65	3.64	8.98	0.03	0.03	1.7
RSKactin	hCof	−1	0	True	0.08	4.12	4.02	−2.32	0.17	0.16	8.99	0.03	0.03	1.72
RSKactin	hCof	−1	0	False	0.1	4.17	4.04	−2.32	0.17	0.16	8.99	0.03	0.03	1.72
RSKactin	hCof	0	2	True	−1.31	1.79	1.3	−0.47	0.47	0.51	9	0.04	0.04	1.75
RSKactin	hCof	0	4	False	−0.74	0.52	0.7	−0.08	0.63	0.39	9	0.04	0.04	1.77
RSKactin	hCof	−2	0	True	−1.26	1.22	1.94	−1.28	1.1	1.11	9	0.03	0.03	1.79
RSKactin	hCof	−3	1	True	−1.24	1.9	1.67	−1.15	0.77	1.38	9.03	0.04	0.04	1.84
RSKactin	hCof	−2	2	True	1.12	2.09	1.43	−1.72	0.32	0.39	9.04	0.05	0.11	1.87
RSKactin	hCof	−1	2	False	−0.56	2.68	2.98	−0.88	1.24	1.04	9.02	0.04	0.04	1.89
RSKactin	hCof	−2	1	True	−1.17	1.4	3.05	−1.51	0.27	1.25	9.02	0.04	0.04	1.89
RSKactin	hCof	−1	2	True	−0.36	2.88	2.93	−0.98	1.38	1.15	9.02	0.04	0.04	1.9
RSKactin	hCof	−3	1	False	−1.26	2.03	1.67	−1.24	0.68	1.43	9.03	0.04	0.05	1.94
RSKactin	hCof	−2	2	False	−1.75	2.21	2.9	−0.45	1.52	0.86	9.03	0.04	0.05	1.95
RSKactin	hCof	−4	0	False	−1.46	2.43	2.65	−0.61	1.5	1	9.03	0.04	0.05	1.96
RSKactin	hCof	0	1	True	−0.09	3.98	4.11	−1.33	0.1	0.1	8.98	0.03	0.03	1.99
RSKactin	hCof	0	1	False	−0.03	4.04	4.05	−1.33	0.1	0.1	8.98	0.03	0.03	1.99
RSKactin	hCof	−3	0	True	−0.95	1.9	2.25	−1.24	1.19	1.31	9.01	0.04	0.04	2
RSKactin	hCof	0	3	False	1.23	1.48	3.52	−1.38	1.2	0.78	9.04	0.06	0.12	2.02
RSKactin	hCof	−4	0	True	−0.38	2.07	1.95	−0.98	1.56	1.57	9.04	0.05	0.05	2.02
RSKactin	hCof	−3	0	False	−1.11	2.12	2.34	−1.4	1.09	1.44	9.02	0.04	0.05	3.13
RSKactin	hCof	0	3	True	−1.47	2.42	2.42	−0.57	0.64	0.68	9.01	0.04	0.06	4.79
RSKactin	hCof	0	4	True	−1.34	1.45	2.25	−0.42	0.81	0.78	9.03	0.05	0.06	12.92

TABLE I. (*Continued.*)

Actin	Cofilin	L	R	Both inclusive?	Q	dQ−	dQ+	W	dW−	dW+	J	dJ−	dJ+	Reduced χ^2
RSKactin	hCof	0	0	False	0.01	4.09	4.07	0.15	4.14	4.01	8.73	0.03	0.03	32.79
RSKactin	hCof	0	0	True	−0.03	4.12	4.14	−0.2	3.99	4.23	8.73	0.03	0.03	32.79
A167EyActin	hCof	0	2	True	−2.14	1.19	1.1	−0.06	0.35	0.29	9.29	0.24	0.22	0.64
A167EyActin	hCof	0	3	True	−1.95	1.47	1.49	−0.1	0.4	0.33	9.29	0.24	0.22	0.65
A167EyActin	hCof	−2	0	True	−2.06	0.83	0.85	−0.2	0.73	0.5	9.29	0.24	0.22	0.66
A167EyActin	hCof	−3	0	True	−1.95	1.1	1.24	−0.2	0.79	0.53	9.29	0.24	0.22	0.68
A167EyActin	hCof	−3	0	False	−1.97	1.15	1.19	−0.24	0.94	0.55	9.31	0.25	0.26	0.69
A167EyActin	hCof	−1	2	True	−1.58	1.52	1.83	−0.28	0.79	0.51	9.3	0.24	0.22	0.7
A167EyActin	hCof	−1	2	False	−1.55	1.51	1.78	−0.28	0.77	0.51	9.29	0.24	0.22	0.7
A167EyActin	hCof	−4	0	False	−1.74	1.4	1.75	−0.25	0.93	0.56	9.3	0.25	0.23	0.72
A167EyActin	hCof	−1	3	False	−1.45	1.68	2.26	−0.27	0.8	0.49	9.3	0.24	0.23	0.74
A167EyActin	hCof	−1	3	True	−1.42	1.69	2.23	−0.28	0.8	0.5	9.3	0.24	0.23	0.75
A167EyActin	hCof	−2	2	False	−1.71	1.45	1.76	−0.34	1.08	0.63	9.32	0.25	0.27	0.77
A167EyActin	hCof	−3	1	True	−2.03	1.24	1.7	−0.32	1.16	0.71	9.31	0.25	0.26	0.83
A167EyActin	hCof	−4	0	True	−0.8	0.95	0.77	−0.38	0.88	0.71	9.3	0.25	0.24	0.85
A167EyActin	hCof	−3	1	False	−1.96	1.29	1.76	−0.4	1.29	0.78	9.32	0.26	0.33	0.89
A167EyActin	hCof	−1	1	True	0.22	4.22	3.95	−1.24	0.23	0.25	9.26	0.25	0.22	1.03
A167EyActin	hCof	−1	1	False	0.29	4.29	3.8	−1.24	0.25	0.25	9.26	0.25	0.24	1.03
A167EyActin	hCof	−2	2	True	−1.1	1.44	1.44	−0.93	0.62	0.74	9.29	0.25	0.36	1.06
A167EyActin	hCof	0	4	True	−0.92	1.17	0.85	−0.18	0.43	0.42	9.28	0.27	0.24	1.07
A167EyActin	hCof	0	3	False	1.74	1.25	3.45	−1.52	1.06	0.67	9.4	0.27	0.29	1.09
A167EyActin	hCof	−2	1	False	−0.07	4.08	4.12	−1.38	0.3	0.31	9.25	0.25	0.23	1.11
A167EyActin	hCof	0	4	False	0.34	0.69	0.76	−0.89	0.81	0.56	9.32	0.3	0.24	1.26
A167EyActin	hCof	−2	1	True	−1.25	1.6	5.5	−1.32	0.43	1.37	9.35	0.26	0.31	1.52
A167EyActin	hCof	−2	0	False	0.04	4.05	4.04	−1.63	0.38	0.4	9.16	0.26	0.23	1.58
A167EyActin	hCof	−1	0	True	−0.02	4.08	4.08	−1.83	0.41	0.46	9.11	0.27	0.24	1.93
A167EyActin	hCof	−1	0	False	0.03	4.12	4.06	−1.83	0.4	0.46	9.11	0.27	0.24	1.94
A167EyActin	hCof	0	2	False	−0.5	3.76	3.78	−0.36	3.79	3.75	8.95	0.27	0.24	2.04
A167EyActin	hCof	0	1	True	0.1	4.11	3.98	−0.88	0.27	0.28	8.95	0.27	0.24	2.38
A167EyActin	hCof	0	1	False	0	4.09	4.07	−0.88	0.26	0.28	8.95	0.26	0.24	2.38
A167EyActin	hCof	0	0	False	0.04	4.1	4.06	0.15	4.18	4	8.2	0.14	0.13	3.32
A167EyActin	hCof	0	0	True	−0.16	3.97	4.15	0.13	4.17	4.05	8.2	0.13	0.13	3.32

B. Actin filament lengths

Actin filaments equilibrated with various concentrations of cofilin for at least one hour were imaged under a total-internal-reflection-fluorescence (TIRF) microscopy system equipped with a 100× objective (Olympus) and Andor iXon897 EM-CCD camera. The recorded analog actin filament images were enhanced by ImageJ software (NIH, USA) and then digitally reconstructed and analyzed with custom-written *Persistence* software [29] (available as a free download at Ref. [30]). Average filament (contour) lengths were determined from the population mean, determined from >20 images with $n = 200 − 500$ filaments. Cofilin binding densities were determined from the binding affinities and protein concentrations [22,26].

C. Model fitting

All of the models considered here have cofilin partition function (Z) of the form

$$Z = e^{-\beta J(L-1)} \sum_{\{s_i\}} e^{-\beta H(\{s_i\})}. \tag{15}$$

This sum involves 2^L terms and is difficult to solve at large L. Fortunately, the partition function can be efficiently processed even at large L when written in the transfer matrix formalism:

$$Z = e^{-\beta J(L-1)} \sum_{\{s_i\}} M_L G^{L/b-1} M_R, \tag{16}$$

where M_L and M_R define the boundary conditions, G is the transfer matrix, and b is the number of sites blocked into the transfer matrix. Note that when $b \neq 1$, M_L and M_R depend on L, as the system may not evenly divide into blocks of size b. We have written a software package for numerically evaluating Eq. (16) on large systems. This is available with a GPLv3 license at github.com/adamjermyn/TransferMatrix.

The cofilin binding density-dependence of the mean filament length was fitted to Eq. (12) using a Markov chain Monte Carlo method [31] with Q, W, and J as unconstrained (i.e., floating) fitting parameters. The term P captures contributions from both the cofilin-actin binding energy and the chemical potential of free cofilin in solution, and thus varies with the cofilin concentration. By numerically solving the equation for the binding fraction, θ, as a function of P:

$$\theta = \frac{1}{Z} \sum_{\text{states}} \frac{1}{L} \sum_i s_i e^{-\beta H} = \beta^{-1} \frac{\partial \ln Z}{\partial P}, \tag{17}$$
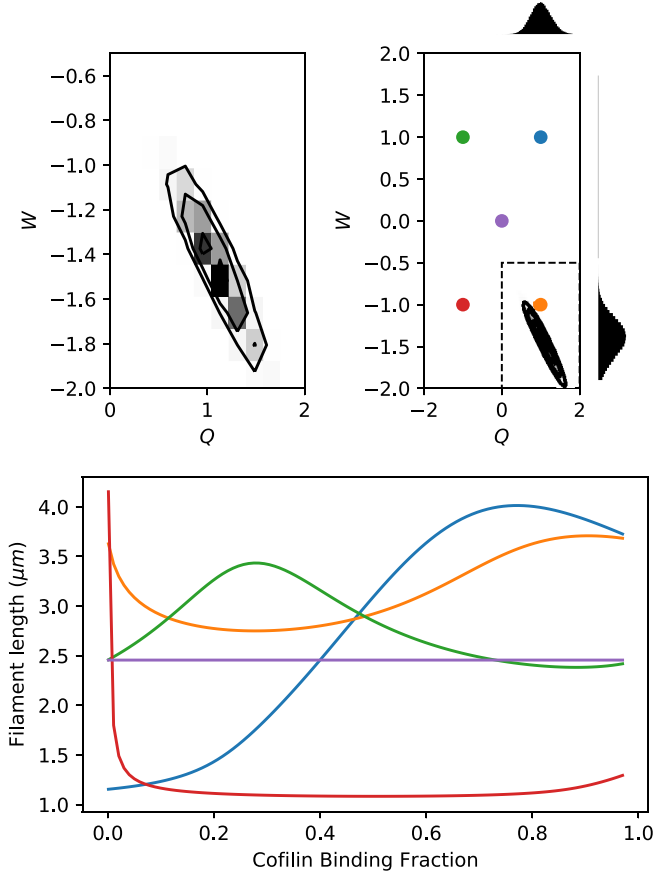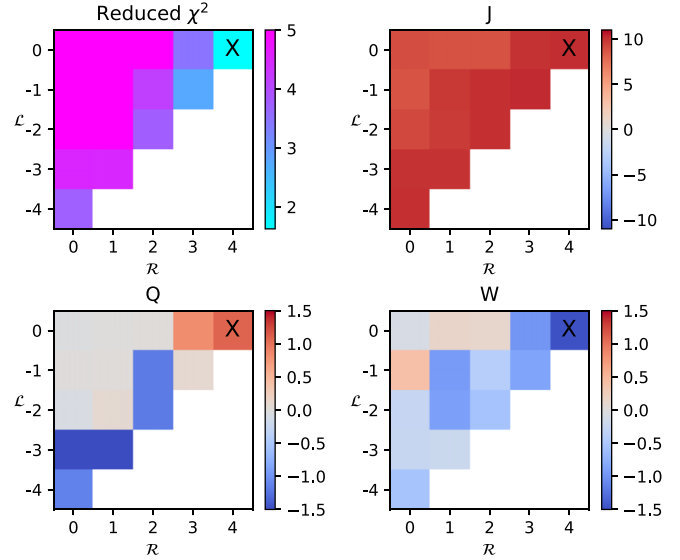
FIG. 4. Best fits of experimental data to all ranges and asymmetries. For each candidate ($\mathcal{L}, \mathcal{R}$), the best fit to D34CyCof severing RSKactin data is chosen from exhaustive analytical computation of the partition function in parameter space (Fig. 3). Q, W, and J are given in units of $k_B T$. We note that in some models Q decouples from the model because, when only a single out-of-plane interaction is included, Q just serves to shift P and so does not actually enter the Hamiltonian. The reduced χ^2 values for these models have been corrected to account for this omission. The best-fitting model by a significant margin is ($\mathcal{L}, \mathcal{R}$)= (0, 4], as can be seen by the low reduced χ^2 value for this model in the top-left panel.

FIG. 3. Uniqueness of best fit parameters. *Top left*: The posterior distribution produced by the Markov chain Monte Carlo fit (Fig. 2 Bottom panel solid green line) of the long-range maximally asymmetric model (0,4] to the D34CyCof severing RSKactin data is shown in grayscale and with contours denoting the regions corresponding to confidence levels of 1σ, 2σ, and 3σ. *Top right*: The same distribution is shown in a wider view of the parameter space. The extent of the top-left portion is shown in a dashed box. The marginal distributions of Q and W are displayed outside the axes, showing that the parameter region within the dashed box is a unique best fit. Q and W terms are in units of $k_B T$. To show the behavior range accessible to the Hamiltonian, five colored points are marked which correspond to the curves shown in the bottom half. *Bottom*: The predicted filament length is shown as a function of cofilin binding fraction for the five different points in parameter space marked on the top-right panel (colors correspond between the panels). While very different behaviors are exhibited by different parts of parameter space, the correct model converges and is quite fundamentally constrained within a narrow parameter space, consistent with a unique solution.

we determined P independently for each data and *(Q, W, J)* set using the BrentQ method [32].

To fit the experimental data, we calculated cofilin binding density dependence of the average actin filament length from the model evaluated here [Fig. 1 and Eq. (12)] using three adjustable parameters J, Q, and W. According to Eqs. (1)–(3), the average actin filament length depends only on scission energy γ. The procedure to calculate γ from the model followed the following steps. First, we choose random initial values of J, Q, and W. We then calculated the individual cofilin binding energy parameter P for every cofilin binding density

using Eq. (17). Second, we computed the L-dependence of the free energy (F) directly from the dominant eigenvalue of the transfer matrix (G; Eq. (16)) with these calculated P values for the different cofilin binding densities. Third, the free energy was computed directly with Eq. (16) for a system with $L = 50$. Combining this with the L-dependence of the free energy we obtained the intercept of the linear relation $F = \alpha L + \gamma$, which yielded the scission energy γ from the intercept of line fit. Fourth, the average actin filament length can be evaluated by Eqs. (2) and (3) from γ. Last, the Markov Chain Monte Carlo search was used to optimize the fit over J, Q, and W.

V. RESULTS AND DISCUSSION

We measured the mean actin filament length as a function of cofilin binding density for three actin-cofilin isoforms, corresponding to different mutational variants of these proteins from different organisms. They are (See Fig. 2 bottom inset): yeast cofilin (D34CyCof) with vertebrate actin (rabbit skeletal, RSKactin), vertebrate cofilin (human cofilin-1, hCof) with yeast actin (A167E), and vertebrate cofilin (hCof) with vertebrate actin (RSKactin). Note that for all mutational variants (Fig. 2 bottom inset), the actin filament length is a nonmonotonic function of cofilin binding density. This suggests a fundamental set of allosteric interactions common across actin and cofilin, with mutational variants changing the depth and shape of the cofilin-binding response curve. Plots of the best fits to the candidate forms of the Hamiltonian are shown for yeast cofilin bound to vertebrate actin (Fig. 2,
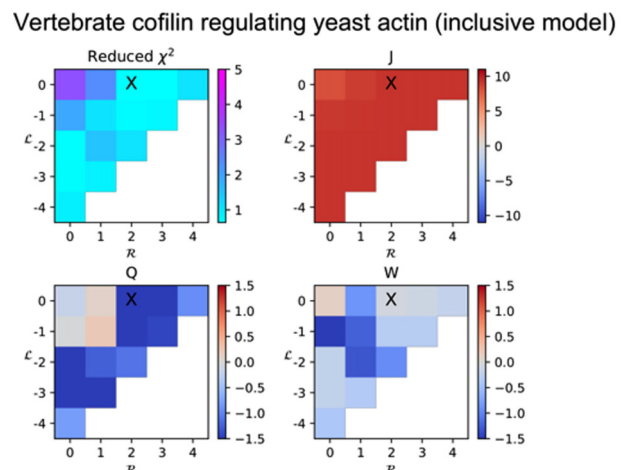
Vertebrate cofilin regulating yeast actin

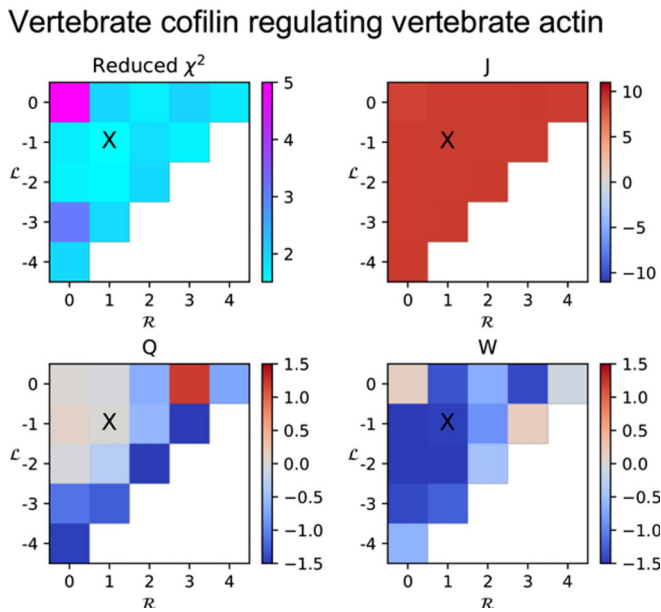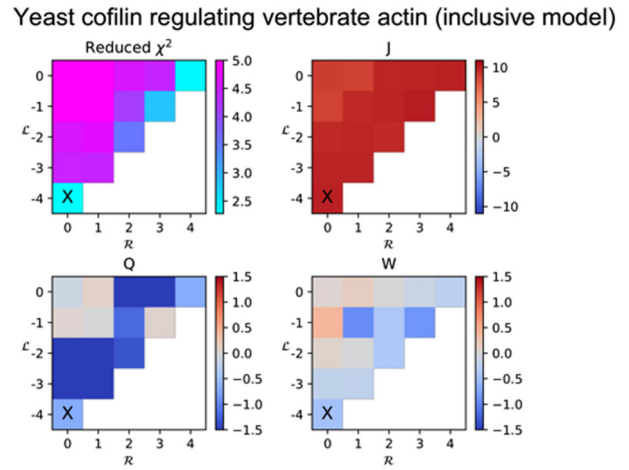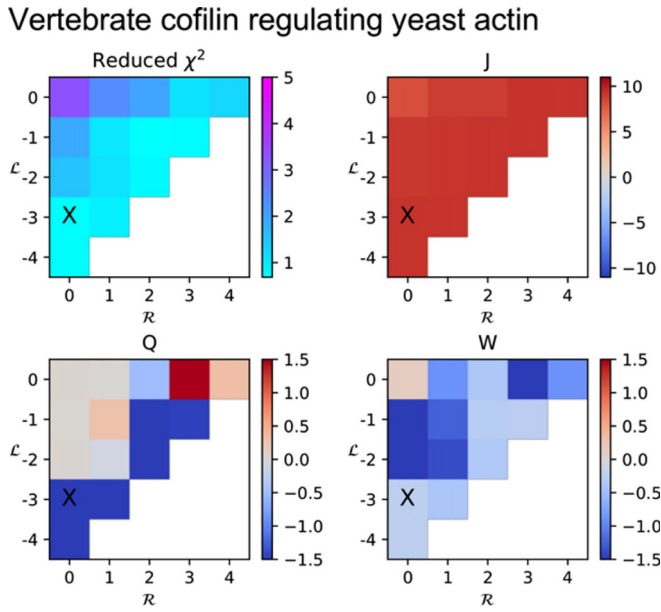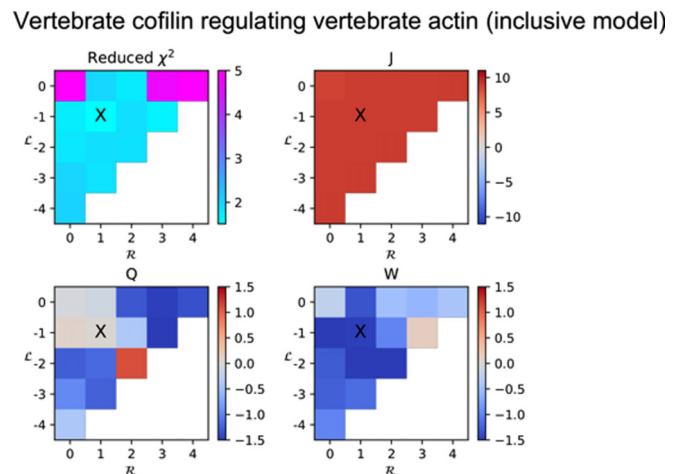## Vertebrate cofilin regulating vertebrate actin

FIG. 5. Mutational variation can significantly alter the allosteric pattern. The same as Fig. 4 for two other cofilactin mutational variants, showing that different mutants can alter the range, asymmetry, and sign of the allosteric interactions.

FIG. 6. Fits using the inclusive model. The same as Figs. 4 and 5, except all longitudinal interactions at the boundaries defined by the lateral interactions are included. The best fit ranges, and asymmetries coincide with the one-sided exclusive model.

bottom), with the results of the fits for all isoforms shown in subsequent figures.

Cofilin binding promotes filament fragmentation, reducing the mean filament length. Maximum severing activity occurs when filaments are half-saturated with cofilin (Fig. 2, bottom). As a result, the mean actin filament length shortens with cofilin occupancy up to a binding density of 0.5, above which the filament length increases with cofilin occupancy (Fig. 2, bottom), consistent with previous findings [27,33–38].

To evaluate the thermodynamic origins of actin filament length regulation by cofilin, we fit the theory to the measured data as described in the methods section. We evaluate the

ability of various ranges (i.e., number of subunits affected; Range from 0 to 4) and directional asymmetry (0 to Range in both directions) of cofilin binding on filament subunit interfaces to account for the equilibrium filament length over a broad range of cofilin binding densities (Fig. 2, lower). As discussed in the theory section, although the fully inclusive

models have comparable fits in some cases, we focus on models which are inclusive of Q on one side and exclusive on the other. For each variant, Range, and Asymmetry, the mean length as a function of cofilin binding was calculated over the entire parameter space. For each isoform, there is a minimum range required to capture the qualitative shape of the data (i.e., the nonmonotonic cofilin dependence) and a higher threshold range required to fit the data quantitatively. In all cases, the fits show a clear preference for range of at least this higher threshold; in most cases, the maximal asymmetry model was also the best fit (see Figs. 4 and 5 for full set of one-sided exclusive model fits). The magnitude of the range and asymmetry remained unchanged in the totally inclusive model (Fig. 6).

For yeast cofilin severing of vertebrate actin filaments (Fig. 2, bottom), an allosteric modulation range of $\geqslant 3$ is needed to qualitatively produce the nonmonotonic (i.e., reduction followed by recovery) cofilin binding density-dependence of the filament length. Ranges less than 3 yield monotonic dependencies (Fig. 2, bottom). A minimal range of 4 and asymmetry of 4 is needed for a good quantitative fit of the experimental data, as indicated by the reduced χ^2 value near unity and the narrowest and most symmetric $\pm 1 - \sigma$ confidence intervals for each parameter (see Table I). The global fit for the Range 4 model (with one side being inclusive), like all ranges investigated, yields a unique solution (Figs. 3 and 4). The model of the best fit is (0, 4].

For vertebrate cofilin severing yeast actin, the best fit with one side exclusive requires a range of 3 and asymmetry of either -4 or 1 ((−3, 0] and (−1, 2], Fig. 5, top); however, several other options are present with comparable reduced χ^2 values, which makes specific conclusions about the Range and Asymmetry of this mutational isoform difficult to draw. In general, the well-fit models favor shorter-ranged and less-asymmetric interactions than for yeast cofilin severing vertebrate actin. Likewise vertebrate cofilin severing vertebrate actin has a range of 2 and asymmetry of 0 ([−1, 1]), though again several other options are present with comparable reduced χ^2 values. Nevertheless, all systems studied require beyond-nearest-neighbor allostery (range $\geqslant 2$; Fig. 5, bottom).

The fits of the data to the theory show that cofilin binding induces long-range changes in actin-actin interaction energies, and that these allosteric changes can propagate either symmetrically or asymmetrically along the filament, depending on the mutational isoform. For yeast cofilin severing vertebrate actin, these changes affect four vacant neighboring binding sites at $i + 1, \ldots, i + 4$, equivalent to six interfaces (4 lateral W and 2 longitudinal Q interactions, in which the latter is inclusive on one side only). For vertebrate cofilin severing yeast actin, the changes affect 3 empty neighboring binding sites at $i, \ldots, i + 2$ or $i - 3, \ldots, i - 1$, equivalent to 5 interfaces (3 lateral W and 2 longitudinal Q). Finally, vertebrate cofilin binding to vertebrate actin affects 2 empty neighboring binding sites at $i - 1$ and $i + 1$, one at each side of a bound coflin, equivalent to 3 interfaces (2 lateral W and 1 longitudinal Q). In this case, the affected empty neighboring cofilin sites are nearest neighbors and symmetric, consistent with an Ising lattice model with nearest neighbor ligand binding cooperativity used for experimental data analysis [22,26]. All these predicted allosteric ranges coincide well with the observed, cofilin-linked

changes in filament twist [35], suggesting that alterations in filament twist are a consequence of these cooperative binding interactions.

The terms in our model have a clear physical interpretation. J represents the actin-actin binding energy. Therefore, it directly influences the overall (mean) actin filament length. P corresponds to the cofilin chemical potential and binding energy, which serves to set the cofilin binding fraction. W and Q terms account for perturbations in the lateral and longitudinal actin-actin binding energies, respectively, linked to cofilin occupancy. Positive W and Q values stabilize their respective actin-actin interactions and negative W and Q values destabilize them. In general, a given Range for a single bound cofilin produces more W terms than Q terms, and thus at low cofilin occupancy, the number of contributing W terms exceeds the number of Q terms. However, the addition of a cofilin unit to an adjacent site adds an equivalent number of additional W and Q terms. For yeast cofilin severing vertebrate actin, the best fit is (0, 4] and a singly bound cofilin generates 4 W and only $2Q$, and addition of a cofilin at an adjacent site adds 1 more W and 2 more Q. Therefore, at high cofilin occupancies, the number of Q terms compares to that of W, and when cofilin binding achieves filament saturation, the total number of contributing Q and W terms are equal. In fitting the experimentally observed nonmonotonic cofilin binding density-dependence of the average actin filament length, competition of the W and Q terms allows the fit to capture the minimum in filament length at intermediate cofilin binding fractions and to recover the plateau at high cofilin occupancies.

The best fits of our model to experimental data reveal different severing mechanism for different mutational isoforms of cofilin-actin pairs. The best fits from all three mutational isoforms yielded similar J value $\sim 9 \, k_B T$ that is due to the similar average actin filament length $\sim 5 \, \mu m$ for yeast actin A167EyActin and vertebrate actin (RSKactin) in the absence of cofilin (Fig. 2 bottom inset and Table I). For yeast cofilin severing vertebrate actin (Fig. 4), the best fit indicates that bound cofilin destabilizes lateral filament subunit interactions (negative $W = -1.5$; Fig. 6 and Table I) and stabilizes overall longitudinal actin-actin interactions (positive $Q = 1.1$). Since the W term dominates at low cofilin binding densities, the average filament length decreases due to the destructive contribution of W terms, while at the high cofilin binding densities, stabilization of filament by Q terms gradually counteracts de-stabilization by W terms because the number of Q increases more readily than that of W as the cofilin occupancy increases. The fact that the absolute values of W and Q are similar suggests that W and Q terms play major roles in the U-shaped response of average filament length to different cofilin binding saturation for this cofilin-actin pair.

In contrast, for vertebrate cofilin severing yeast actin (Fig. 5, top) both the best-fit and the several next-best models show that it is the longitudinal actin-actin interfaces that are destabilized (negative $Q \sim -1.6$ to -2.0), while lateral actin-actin interfaces are weakly destabilized (negative $W \sim -0.2$ to -0.3). For vertebrate cofilin severing vertebrate actin (Fig. 5, bottom), both the best-fit and the several next-best models show that the changes in longitudinal interfaces are minor (term $Q \sim 0$), but the lateral actin-actin interfaces are

destabilized (negative $W \sim -1.5$). The regulation of actin filament by Q and W terms in those two cofilin-actin mutational isoforms are similar, i.e., one of them is de-stabilizing and the other has a weak or negligible effect. The appearance of these features across several different well-fitting models indicates that they are robust and not strongly influenced by the precise choice of interaction range and form.

In addition to the distance or magnitude of allostery, which determines the numbers of Q and W terms generated by a single bound cofilin, how the *sign* of allosteric interactions, i.e., stabilizing or destabilizing, can be uniquely determined by fitting of experimental data may be further understood by examining the different curves in Fig. 3, which show all combinations of signs of W and Q. In the regime of negative destabilizing W, a positive stabilizing Q produces a rise at cofilin binding fraction (orange line in Fig. 3), as experimentally observed for one of the mutational isoforms. This is because at low binding fraction, the dominating number of destabilizing W terms are proportional to the density of bound cofilin. At intermediate cofilin binding densities, the different number of W and Q reaches the maximum, so that the average actin filament length falls to a minimum. Above a high enough cofilin binding density, the number of stabilizing Q gradually catches up with the number of destabilizing W and balances it out. For a positive stabilizing W and a negative destabilizing Q, the effect is the opposite and they produce a bell shaped cofilin binding density dependence of average filament length (green line in Fig. 3). When both W and Q are positive stabilizing (blue line) or negative destabilizing (red line in Fig. 3), the response of average filament length to increasing cofilin binding density is monotonically increasing or decreasing with cofilin binding before saturation.

The conclusion from this work will help understanding the different mechanism in regulation of actin filaments by cofilin in different organisms. An interesting observation is that $W \sim -1.5$ in both yeast (D34CyCof) and vertebrate (hCof) severing vertebrate actin (RSKactin), but the Q values differ. This suggests that the lateral interaction between actin subunits in RSKactin actin are weak compared to longitudinal interaction, and that yeast cofilin stabilizes longitudinal actin-actin interaction to a greater extent than human cofilin. The latter behavior is consistent with the 30-fold higher affinity of yeast cofilin for vertebrate actin compared to vertebrate cofilin

[36]. Moreover, comparison of yeast actin (A167EyActin) to vertebrate RSKactin severing by human cofilin suggests that longitudinal actin-actin interaction in yeast actin filaments, as opposed to lateral contacts, are destabilized by cofilin, contributing to different severing pathway mechanisms [27].

These predictions of the energetics and the cooperative nature of actin filament length regulation complement previous structure-based studies carried out with purified protein components. Filament structures obtained by electron microscopy [11,20,23,39,40], molecular dynamics simulations [10,41], and biochemical solution studies [12,13,21,42] indicate that cofilin binds between two longitudinally adjacent actin subunits and alters longitudinal and lateral interfacial structure, including interfaces adjacent to the site of cofilin binding (i.e., nearest neighbors) as well as interfaces that are farther away (i.e., nonnearest neighbors). Therefore, the theoretical framework presented here, in conjunction with micron-scale measurements of filament length, has allowed a quantitative thermodynamic characterization of the range, directionality, and sign of allosteric regulation of actin filaments by cofilin. Because the formalism is general, it is readily applicable to other polymerization processes, both with and without associated regulatory components.

[1] R. Tycko, Molecular structure of amyloid fibrils: insights from solid-state NMR, Q. Rev. Biophys. **39**, 1 (2006).

[2] R. Dominguez and K. C. Holmes, Actin structure and function, Annu. Rev. Biophys **40**, 169 (2011).

[3] A. Matus, Actin-based plasticity in dendritic spines, Science **290**, 754 (2000).

[4] Y. A. Puius, N. M. Mahoney, and S. C. Almo, The modular structure of actin-regulatory proteins, Curr. Opin. Cell Biol. **10**, 23 (1998).

[5] A. Cooper and D. T. F. Dryden, Allostery without conformational change, Eur. Biophys. J. **11**, 103 (1984).

[6] H. N. Motlagh, J. O. Wrabl, J. Li, and V. J. Hilser, The ensemble nature of allostery, Nature **508**, 331 (2014).

[7] B. H. Zimm and J. K. Bragg, Theory of phase transition between helix and random coil in polypeptide chains, J. Chem. Phys. **31**, 526 (1959).

[8] M. LeVine and H. Weinstein, AIM for allostery: using the Ising model to understand information processing and transmission in allosteric biomolecular systems, Entropy **17**, 2895 (2015).

[9] P. van der Schoot, *Supramolecular Polymers* (CRC Press, Boca Raton, FL, 2019).

[10] J. Pfaendtner, E. M. De La Cruz, and G. A. Voth, Actin filament remodeling by actin depolymerization factor/cofilin, Proc. Natl. Acad. Sci. USA **107**, 7299 (2010).

[11] A. McGough and W. Chiu, ADF/cofilin weakens lateral contacts in the actin filament, J. Mol. Biol. **291**, 513 (1999).

[12] A. A. Bobkov, A. Muhlrad, A. Shvetsov, S. Benchaar, D. Scoville, S. C. Almo, and E. Reisler Cofilin(ADF) affects lateral contacts in F-actin, J. Mol. Biol. **337**, 93 (2004).

[13] A. A. Bobkov, A. Muhlrad, D. A. Pavlov, K. Kokabi, A. Yilmaz, and E. Reisler, Cooperative effects of cofilin (ADF) on actin structure suggest allosteric mechanism of cofilin function, J. Mol. Biol. **356**, 325 (2006).

[14] M. E. Cates, Reptation of living polymers: dynamics of entangled polymers in the presence of reversible chain-scission reactions, Macromolecules **20**, 2289 (1987).

[15] F. Oosawa, *Thermodynamics of the Polymerization of Protein*, (Academic Press, San Diego, CA, 1975).

[16] L. Edelstein-Keshet, Models for the length distributions of actin filaments: I. Simple polymerization and fragmentation, Bull. Math. Biol. **60**, 449 (1998).

[17] D. Sept, J. Xu, T. D. Pollard, and J. A. McCammon, Annealing accounts for the length of actin filaments formed by spontaneous polymerization, Biophys. J. **77**, 2911 (1999).

[18] T. D. Pollard and W.C. Earnshaw, *Cell Biology*, (Saunders, Philadelphia, PA, 2007).

[19] E. M. De La Cruz and E. M. Ostap, *Actin in Cells* (Jones & Bartlett Publishing, Burlington, MA, 2013).

[20] A. McGough, B. Pope, W. Chin, and A. Weeds, Cofilin changes the twist of F-actin: Implications for actin filament dynamics and cellular function, J. Cell Biol. **138**, 771 (1997).

[21] I. V. Dedova, O. P. Nikolaeva, V. V. Mikhailova, C. G. dos Remedios, and D. I. Levitsky. Two opposite effects of cofilin on the thermal unfolding of F-actin: a differential scanning calorimetric study, Biophys. Chem. **110**, 119 (2004).

[22] E. M. De La Cruz. Cofilin binding to muscle and nonmuscle actin filaments: isoform-dependent cooperative interactions, J. Mol. Biol. **346**, 557 (2005).

[23] A. Heuhn, W. Cao, W. A. Elam, X. Liu, E. M. De La Cruz, and C. V. Sindelar, The actin filament twist changes abruptly at boundaries between bare and cofilin-decorated segments, J. Biol. Chem. **293**, 5377 (2018).

[24] K. X. Ngo, N. Kodera, E. Katayama, T. Ando, and T. Q. Uyeda, Cofilin-induced unidirectional cooperative conformational changes in actin filaments revealed by high-speed atomic force microscopy, eLife **4**, e04806 (2015).

[25] K. Tanaka, S. Takeda, K. Mitsuoka, T. Oda, C. Kimura-Sakiyama, Y. Maéda, and A. Narita, Structural basis for cofilin binding and actin filament disassembly, Nat Commun. **9**, 1860. (2018).

[26] W. Cao, J. Goodarzi, and E. M. De La Cruz, Energetics and kinetics of cooperative cofilin-actin filament interactions. J. Mol Biol. **361**, 257 (2006).

[27] H. Kang, M.J. Bradley, W. Cao, K. Zhou, E. E. Grintsevich, A. Michelot, C. V. Sindelar, M. Hochstrasser, and E. M. De La Cruz, Site-specific cation release drives actin filament severing by vertebrate cofilin, Proc. Natl. Acad. Sci. USA **111**, 17821 (2014).

[28] B. R. McCullough, E. E. Grintsevich, C. K. Chen, H. Kang, A. L. Hutchison, A. Henn, W. Cao, C. Suarez, J. L. Martiel, L. Blanchoin, E. Reisler, and E. M. De La Cruz, Cofilin-linked changes in actin filament flexibility promote severing, Biophys. J. **101**, 151 (2011).

[29] J. S. Graham, B. R. McCullough, H. Kang, W. A. Elam, W. Cao, and E. M. De La Cruz, Multi-platform compatible software for analysis of polymer bending mechanics, PLoS One **9**, e94766 (2014).

[30] delacruzlab.yale.edu.

[31] D. Foreman-Mackey, D. W. Hogg, D. Lang, and J. Goodman, emcee: The MCMC Hammer, Proc. Ast. Soc. Pacific. **125**, 306 (2013).

[32] R. P. Brent, An Algorithm with Guaranteed Convergence for Finding a Zero of a Function, in *Algorithms for Minimization without Derivatives* (Prentice-Hall, Englewood Cliffs, NJ, 1973), Chap. 4.

[33] D. Pavlov, A. Muhlrad, J. Cooper, M. Wear, and E. Reisler, Actin filament severing by cofilin, J Mol. Biol. **365**, 1350 (2007).

[34] E. M. De La Cruz, How cofilin severs an actin filament, Biophys. Rev. **1**, 51 (2009).

[35] B. R. McCullough, L. Blanchoin, J. L. Martiel, and E. M. De La Cruz, Cofilin increases the bending flexibility of actin filaments: Implications for severing and cell mechanics, J. Mol. Biol. **381**, 550 (2008).

[36] C. Suarez, J. Roland, R. Boujemaa-Paterski, H. Kang, B. R. McCullough, A. C. Reymann, C. Guérin, J. L. Martiel, E. M. De La Cruz, and L. Blanchoin, Cofilin tunes the nucleotide state of actin filaments and severs at bare and decorated segment boundaries, Curr. Biol. **21**, 862 (2011).

[37] W. A. Elam, H. Kang, and E. M. De La Cruz, Biophysics of actin filament severing by cofilin, FEBS Lett. **587**, 1215 (2013).

[38] W. A. Elam, W. Cao, H. Kang, A. Huehn, G. M. Hocky, E. Prochniewicz, A. C. Schramm, K. Nieves-Torres, J. Garcia, T. Bonello, T. Fath, P. W. Gunning, D. D. Thomas, G. A. Voth, C. V. Sindelar, and E. M. De La Cruz, Phosphomimetic S3D cofilin binds but only weakly severs actin filaments, J. Biol. Chem. **292**, 19565 (2017).

[39] V. E. Galkin, A. Orlova, N. Lukoyanova, W. Wriggers, and E. H. Egelman, Actin depolymerizing factor stabilizes and existing state of F-actin and can change the tilt of F-actin subunits, J. Cell Biol. **153**, 75 (2001).

[40] V. E. Galkin, A. Orlova, D. S. Kudryashov, A. Solodukhin, E. Reisler, G. Schroder, and E. H. Egelman, Remodeling of actin filaments by ADF/cofilin proteins, Proc. Natl. Acad. Sci. USA **108**, 20568 (2011).

[41] J. Fan, M. G. Saunders, E. J. Haddadian, K. F. Freed, E. M. De La Cruz, and G. A. Voth, Molecular origins of cofilin-linked changes in actin filament mechanics, J. Mol. Biol. **425**, 1225 (2013).

[42] A. A. Bobkov, A. Muhlrad, K. Kokabi, S. Vorobiev, S. C. Almo, and E. Reisler, Structural effects of cofilin on the longitudinal contacts in F-actin, J. Mol. Biol. **323**, 739 (2002).